



HAL
open science

Electroosmotic Coupling in Porous Media, a New Model Based on a Fractal Upscaling Procedure

Luong Duy Thanh, Damien Jougnot, Phan van Do, Aida Mendieta, Nguyen Xuan Ca, Vu Xuan Hoa, Pham Minh Tan, Nguyen Thi Hien

► **To cite this version:**

Luong Duy Thanh, Damien Jougnot, Phan van Do, Aida Mendieta, Nguyen Xuan Ca, et al.. Electroosmotic Coupling in Porous Media, a New Model Based on a Fractal Upscaling Procedure. *Transport in Porous Media*, 2020, 134 (1), pp.249-274. 10.1007/s11242-020-01444-7 . hal-02950764

HAL Id: hal-02950764

<https://hal.sorbonne-universite.fr/hal-02950764>

Submitted on 30 Sep 2020

HAL is a multi-disciplinary open access archive for the deposit and dissemination of scientific research documents, whether they are published or not. The documents may come from teaching and research institutions in France or abroad, or from public or private research centers.

L'archive ouverte pluridisciplinaire **HAL**, est destinée au dépôt et à la diffusion de documents scientifiques de niveau recherche, publiés ou non, émanant des établissements d'enseignement et de recherche français ou étrangers, des laboratoires publics ou privés.

1 Electroosmotic coupling in porous media, a new 2 model based on a fractal upscaling procedure

3 Luong Duy Thanh^a, Damien Jougnot^b, Phan Van Do^a, Aida Mendieta^b,
4 Nguyen Xuan Ca^c, Vu Xuan Hoa^c, Pham Minh Tan^d, Nguyen Thi Hien^{e,f,*}

5 *^aThuyloi University, 175 Tay Son, Dong Da, Hanoi, Vietnam*

6 *^bSorbonne Université, CNRS, EPHE, UMR 7619 Metis, F-75005, Paris, France*

7 *^cFaculty of Physics and Technology, TNU-University of Sciences, Thai Nguyen, Vietnam*

8 *^dFaculty of Fundamental Sciences, Thai Nguyen University of Technology, Thai Nguyen,*

9 *Vietnam*

10 *^eCeramics and Biomaterials Research Group, Advanced Institute of Materials Science,*

11 *Ton Duc Thang University, Ho Chi Minh City, Vietnam*

12 *^fFaculty of Applied Sciences, Ton Duc Thang University, Ho Chi Minh City, Vietnam*

13 Abstract

Electrokinetic and electroosmotic couplings can play important roles in water and ions transport in charged porous media. Electroosmosis is the phenomena explaining the water movement in a porous medium subjected to an electrical field. In this work, a new model is obtained through a new up-scaling procedure, considering the porous medium as a bundle of tortuous capillaries of fractal nature. From the model, the expressions for the electroosmosis pressure coefficient, the relative electroosmosis pressure coefficient, the maximum back pressure, the maximum flow rate, the flow rate-applied back pressure relation and the product of the permeability and formation factor of porous media are also obtained. The sensitivity of the relative electroosmosis pressure coefficient is then analyzed and explained. The model predictions are then successfully compared with published datasets. Additionally, we deduce an expression for the relative streaming potential coefficient and then compare it with a previously published model and experimental data from a dolomite rock sample. We find a good agreement between those models and experimental

data, opening up new perspectives to model electroosmotic phenomena in porous media saturated with various fluids.

14 *Keywords:* Electroosmosis; Electrokinetics; Water saturation; Zeta
15 potential; Fractal; Porous media

*Corresponding author

June 26, 2020

Email address: nguyenthien@tdtu.edu.vn (Nguyen Thi Hien)

16 **1. Introduction**

17 Electroosmosis is one of the effects of electrokinetic phenomena that occur in porous media with surface charges when filled with one or more fluids containing charged particles. It arises due to the induced movement of a liquid by a voltage across a porous sample and is directly linked to an electrical double layer between the solid grain surface and the pore solution. Electroosmosis has been studied both experimentally and theoretically for a long time (e.g., Reuss, 1809; Quincke, 1861; Smoluchowski, 1902; Nourbehecht, 1963; Lyklema, 1995). Electroosmotic flow is a critical phenomenon that is used in a variety of applications. For example, electroosmotic flow pumps have been used in different fields of microfluidics such as biological and chemical analysis (Good et al., 2006), liquid drug reagent injection/delivery (e.g., Tsai & Sue, 2007; Wang et al., 2009), microelectronic chip cooling (e.g., Linan Jiang et al., 2002; Singhal et al., 2004) and microfluidic devices (e.g., Hu & Li, 2007; Bruus, 2008; Kirby, 2010). Solutes and nonaqueous phase liquids/dense nonaqueous phase liquids can be removed by an electroosmotic technique in the vadose zone for remediation purposes (e.g., Bruell et al., 1992; Wise & Tran, 1994; Han et al., 2004; Reddy et al., 1997). Additionally, electroosmosis has great potential for the dewatering of earth masonry structures (e.g., Casagrande, 1983; Lockhart & Hart, 1988; Larue et al., 2006) or drying moisture ingress in existing buildings, stone and earth masonry structures (e.g., Lockhart & Hart, 1988; Ottosen & Rørig-Dalgaard, 2006; Bertolini et al., 2009).

38
39 Many studies on electroosmosis flow reported in the literature use cylindrical capillaries or microchannels between two parallel plates (e.g., Rice & Whitehead, 1965; Levine et al., 1975; Olivares et al., 1980; Ohshima & Kondo, 1990; Mohiuddin Mala et al., 1997; Vennela et al., 2011). In

porous ⁴³media, electroosmotic flow has been presented using capillary bundle models ⁴⁴with different capillary geometry such as rectangular, cylindrical and annular ⁴⁵geometries (e.g., Wu & Papadopoulos, 2000; Pascal et al., 2012). Bandopad⁴⁶hyay et al. (2013) introduced the parameter of the electro-permeability that ⁴⁷relates the flow rate with the applied voltage in porous media. Based on ⁴⁸the electroosmotic flow in a single capillary, models for the height difference ⁴⁹between the U-tube experiment caused by electroosmosis in a fully saturated ⁵⁰porous medium were presented (e.g., Paillat et al., 2000; Liang et al., 2015). ⁵¹For characterization of electroosmotic miropumps fabricated by packing non⁵²porous silica particles, a bundle of capillary tubes model was applied (e.g., ⁵³Zeng et al., 2001; Yao & Santiago, 2003). Besides capillary tubes models, ⁵⁴other approaches based on volume-averaging upscaling can be also applied ⁵⁵to calculate the electrokinetic coupling in porous media (e.g., Pride, 1994; ⁵⁶Revil & Linde, 2006; Revil et al., 2007).

⁵⁷It has been shown that natural porous media have fractal properties. ⁵⁸Their pore space is statistically self-similar over several length scales (among ⁵⁹many others, see Mandelbrot, 1982; Katz & Thompson, 1985; Yu & Cheng, ⁶⁰2002). Theory on the fractal nature of porous media has attracted much ⁶¹attention in different areas (e.g., Mandelbrot, 1982; Feder & Aharony, 1989). ⁶²Therefore, models based on the fractal theory have been applied to study ⁶³phenomena in both fully and partially saturated porous media (e.g., Cai ⁶⁴et al., 2012a,b; Liang et al., 2014; Guarracino & Jougnot, 2018; Soldi et al., ⁶⁵2019; Thanh et al., 2018, 2019). However, to the best of our knowledge, ⁶⁶the fractal theory has not yet been used to study electroosmosis in a porous ⁶⁷medium under water saturated and partially saturated conditions.

⁶⁸In this work, we apply fractal theory in porous media to obtain a mech⁶⁹anistic analytical model to describe electroosmotic flow in porous media us⁷⁰ing a capillary tube model. From the derived model, the expressions for ⁷¹the electroosmotic pressure coefficient, the relative electroosmosis pressure ⁷²coefficient, the maximum back pressure, the maximum flow rate, the flow ⁷³rate-applied back pressure relation and the product of the formation fac⁷⁴tor and permeability of porous media are also obtained. To validate the ⁷⁵model, the sensitivity of the relative electroosmosis pressure coefficient K_E^r ⁷⁶to irreducible water saturation S_{irr} , ratio of the minimum pore radius to the ⁷⁷maximum pore radius α and fractal dimension for pore space D_f is analyzed ⁷⁸and explained. The model is then compared with published results in both ⁷⁹

cases of full saturation and partial saturation. Additionally, the expression K_S^r for the relative streaming potential coefficient is also deduced from K_E^r . From that, the change of the relative streaming potential coefficient K_S^r with the water saturation is predicted and compared with another model and with experimental data for a dolomite rock sample available in literature.

2. Theoretical background of electroosmosis

2.1. Theory of electroosmosis

Porous media are constituted by minerals (e.g., silicates, oxides, carbonates) or other materials (e.g., polymers, biological materials) that are generally electrically charged due to isomorphous substitutions (e.g., Hunter, 1981;

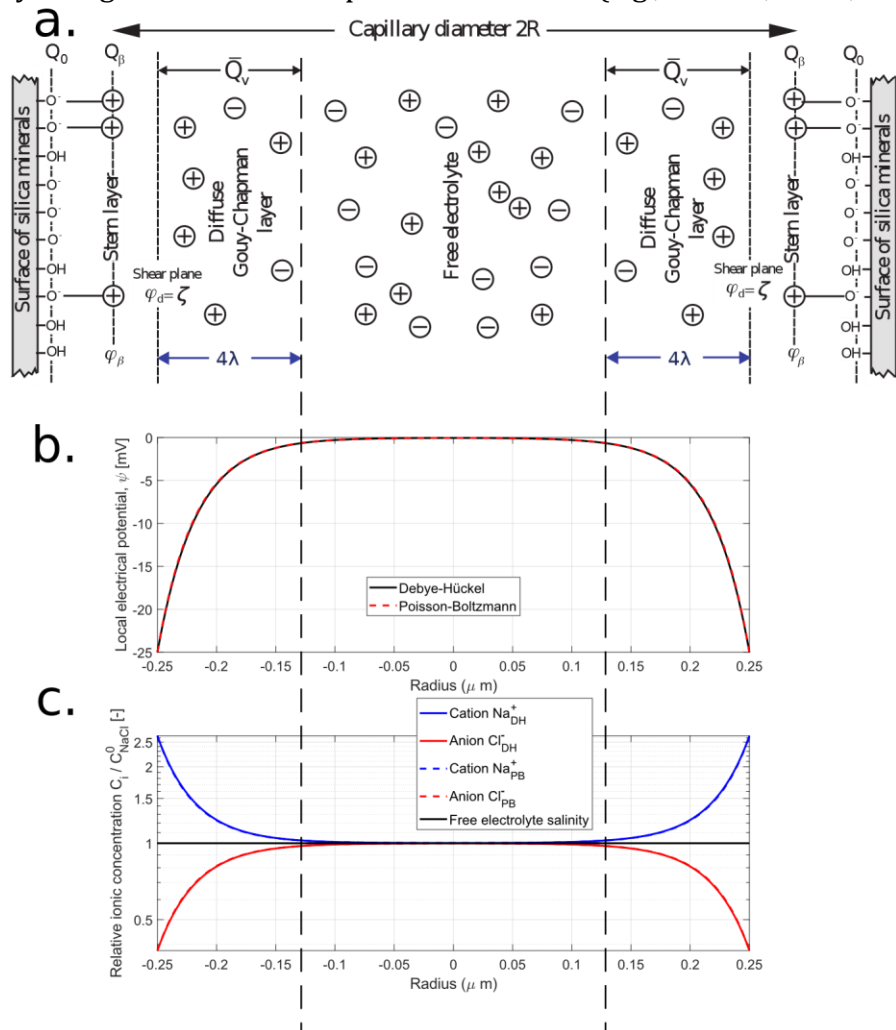


Figure 1: (a) Sketch of the electrical double layer at the surface of a mineral in contact with water. Comparison between the Debye-Hu"ckel (DH) approximation (plain line, Eq. (13)) and the Poisson-Boltzman equation (dashed line) to compute (b) the electrical potential distribution and (c) the ionic species relative concentration distribution in a capillary ($R = 0.25 \mu\text{m}$) containing a NaCl electrolyte with 10^{-4} mol/L (i.e., $\lambda = 0.0304 \mu\text{m}$). Note that the dashed and plain lines are perfectly superimposed, validating the use of Eq. (13).

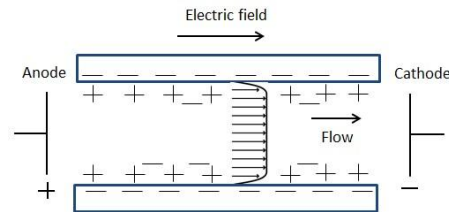


Figure 2: Electroosmosis flow in a capillary tube.

⁸⁹Jacob & Subirm, 2006) as shown in Fig. 1. The pore fluid nearby solid ⁹⁰ solution interface contains an excess of charges (counter-ions) to insure the ⁹¹ electro-neutrality of the entire system. These counter-ions are often cations ⁹² and surface charges are often negatively charged in environmental conditions. ⁹³ Note that the surface charges strongly depend on the pH and that the sign ⁹⁴ can change at low pH. The value at which the sign changes is called the point ⁹⁵ of zero charge (e.g., Hunter, 1981; Leroy & Revil, 2004). This gives rise to ⁹⁶ the charge distribution known as the electrical double layer (EDL) as shown ⁹⁷ in Fig. 1a. The EDL is composed of a Stern layer, where counter-ions are ⁹⁸ adsorbed onto the solid surface and are immobile, and a diffuse layer that ⁹⁹ contains mobile counter-ions and co-ions. In the diffuse layer, the distribu¹⁰⁰ tion of ions and electric potential are governed by the Poisson-Boltzman (PB) ¹⁰¹ equation in quasistatic conditions. The solution to the linear PB equation ¹⁰² for a cylinder is well-known and the electric potential decays over distance ¹⁰³ from the charged surface as displayed in Fig. 1b using the code provided by ¹⁰⁴ Leroy & Mainault (2018). Further away from the solid-solution is the bulk ¹⁰⁵ electrolyte, free from surface charge influence, it contains an equal number ¹⁰⁶ of cations and anions and is therefore electrically neutral (Fig. 1c). The ¹⁰⁷ shear plane or the slipping plane is the closest place to the solid in which ¹⁰⁸ water flow occurs and the electrical potential at this plane is called the zeta ¹⁰⁹ potential (ζ). The zeta potential depends on parameters including mineral ¹¹⁰ composition of porous media, ionic species that are present in the fluid, the ¹¹¹ pH of the fluid, fluid electrical conductivity and temperature etc. (see Hunter ¹¹² (1981); Davis et al. (1978); Jaafar et al. (2009) for more details). ¹¹³ Reuss (1809) carried out the

first experiment on electroosmosis by applying a DC voltage across a water saturated porous sample in a U-tube. When a DC voltage is applied across a capillary containing water, ions in the EDL are submitted to an electric force and move to the electrode of oppo-

site polarity. That leads to the movement of the fluid near the solid surface as well as the bulk liquid due to viscous forces. The net motion of liquid is called electroosmotic flow (Fig. 2). The pressure necessary to counterbalance electroosmotic flow is defined as the electroosmotic pressure (e.g., Jacob & Subirm, 2006).

2.2. Governing equations

The electrokinetic coupling in a fluid saturated porous medium is described by two linear equations (e.g., Li et al., 1995; Pengra et al., 1999)

$$\mathbf{U}_e = -\sigma \nabla V - \Pi_{12} \nabla P. \quad (1)$$

$$\mathbf{U}^f = -\Pi_{21} \nabla V - \frac{k}{\eta} \nabla P, \quad (2)$$

where \mathbf{U}_e and \mathbf{U}^f are the electric current density ($A\ m^{-2}$) and Darcy flux ($m\ s^{-1}$), V is the electrical potential (V), P is the pressure that drives the flow, σ and k are the electrical conductivity ($S\ m^{-1}$) and permeability (m^2) of the porous medium, η is the dynamic viscosity of the fluid, the off-diagonal coefficients (Π_{12} and Π_{21}) are the electrokinetic coupling coefficients. In the

steady state, those coupling coefficients must satisfy the reciprocal relation of Onsager: $\Pi_{12} = \Pi_{21} = \Pi$.

The streaming potential coefficient is defined when the electric current density \mathbf{U}_e is zero (e.g., Li et al., 1995; Wang et al., 2016), leading to

$$K_S = \frac{\Delta V}{\Delta P} = -\frac{\Pi}{\sigma}. \quad (3)$$

Note that another formulation in which streaming potential coefficient for saturated porous media is described through the effective excess charge density \hat{Q}_v (C/m^3) dragged by the flow of the pore water was proposed by (e.g., Revil & Leroy, 2004; Revil & Linde, 2006)

$$K_S = -\frac{\hat{Q}_v k}{\sigma \eta}. \quad (4)$$

138 The electroosmotic pressure coefficient is defined when the Darcy flux
 \mathbf{U}_f
 139 is zero (e.g., Li et al., 1995; Wang et al., 2016), leading to

$$K_E = \frac{\Delta P}{\Delta V} = -\frac{\Pi \eta}{k}. \quad (5)$$

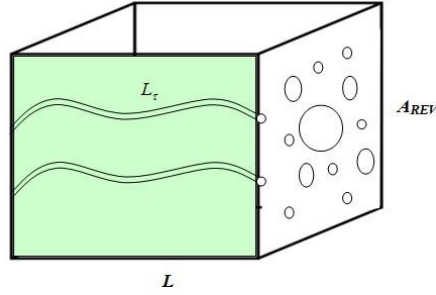


Figure 3: Sketch of the considered conceptual representative elementary volume (REV): Parallel and tortuous capillary tubes with radii following a fractal distribution.

140 By the volume averaging approach, Pride (1994) obtained the steady state
 141 coupling coefficient under a thin electrical double layer
 assumption as

$$\Pi = \frac{\phi \epsilon_r \epsilon_0 \zeta}{\tau \eta} = \frac{\epsilon_r \epsilon_0 \zeta}{F \eta}, \quad (6)$$

142 where ϵ_r is the relative permittivity of the fluid, ϵ_0 is the dielectric per
 143 mittivity in vacuum, ϕ , τ and F are the porosity, hydraulic tortuosity and

144 formation factor of porous media, respectively. Note that the link $\phi F = \tau$
 145 has been used in Eq. (6) (e.g., Wyllie & Rose, 1950; Ghanbarian et al., 2013)

146
 147 Substituting Eq. (6) into Eq. (5), one obtains

$$K_E = -\frac{\epsilon_r \epsilon_0 \zeta}{F k}. \quad (7)$$

148 In this work, we will obtain the analytical models for K_E as well as other
 149 quantities based on a fractal upscaling approach instead of the volume
 aver₁₅₀aging approach for partially saturated porous media.

151 3. Model development

152 *3.1. Electrical potential distribution at pore scale*

153 Consider binary symmetric 1:1 electrolytes (e.g., NaCl) of bulk ionic concentration C^0 (mol/m³) with an electrical potential $\psi(r)$ (V) at a distance r from the axis. If the excess charge density at this point is $\rho(r)$ (C m⁻³), then the Poisson equation is given by (e.g., Rice & Whitehead, 1965; Gierst, 1966)

$$\frac{1}{r} \frac{d}{dr} \left(r \frac{d\psi(r)}{dr} \right) = -\frac{\rho(r)}{\epsilon_r \epsilon_0}, \quad (8)$$

158 From the Boltzmann equation, the following is obtained

$$\rho(r) = NeC^0 \left[e^{-\frac{e\psi(r)}{k_b T}} - e^{\frac{e\psi(r)}{k_b T}} \right] = 2NeC^0 \sinh \frac{e\psi(r)}{k_b T} \quad (9)$$

159 where k_b is the Boltzmann's constant, T is temperature (in K), N is the Avogadro number and e is the elementary charge.

161 If $\left| \frac{e\psi(r)}{k_b T} \right| \ll 1$ that is called the Debye-Hu"ckel approximation (e.g., Pride,

162 1994; Hunter, 1981; Jougnot et al., 2019), $\sinh \frac{e\psi(r)}{k_b T} \approx \frac{e\psi(r)}{k_b T}$. The Poisson equation now becomes

$$\frac{1}{r} \frac{d}{dr} \left(r \frac{d\psi(r)}{dr} \right) = -\frac{2Ne^2 C^0}{\epsilon_0 \epsilon_r k_b T} \psi(r) \quad (10)$$

164 OR

$$\frac{1}{r} \frac{d}{dr} \left(r \frac{d\psi(r)}{dr} \right) = -\frac{\psi(r)}{\lambda^2} \quad (11)$$

165 where $\lambda = \sqrt{\frac{\epsilon_0 \epsilon_r k_b T}{2Ne^2 C^0}}$ is defined as the Debye length (e.g., Israelachvili, 1992).

166 The boundary conditions of Eq. (11) to be satisfied for the cylindrical capillary surface are (Rice & Whitehead, 1965):

$$\psi(r) = \begin{cases} \psi(R) = \zeta \\ \left. \frac{d\psi(r)}{dr} \right|_{r=0} = 0 \end{cases} \quad (12)$$

168 Under the boundary conditions given by Eq. (12), the analytical solution of $\psi(r)$ and $\rho(r)$ are obtained as (Rice & Whitehead, 1965)

$$\psi(r) = \zeta \frac{I_0\left(\frac{r}{\lambda}\right)}{I_0\left(\frac{R}{\lambda}\right)} \quad (13)$$

170 and

$$\rho(r) = -\frac{\epsilon_0 \epsilon \zeta}{\lambda^2} \frac{I_0\left(\frac{r}{\lambda}\right)}{I_0\left(\frac{R}{\lambda}\right)} \quad (14)$$

171 where I_0 is the zero-order modified Bessel function of the first kind. Figure 1
 172 compares the potential and concentrations of ions in the EDL calculated
 from 173 Eq. (13) and the exact Poisson-Boltzmann solution (see Leroy &
 Mainault 174 (2018) for more details). It shows that Eq. (13) is a correct
 approximation 175 for the Poisson-Boltzmann true solution.

176 3.2. Velocity distribution at pore scale

177 Under application of an electric field E and a fluid pressure difference ΔP
 178 across a tortuous capillary of radius R , the fluid flow is the sum of a
 Poiseuille 179 flow generated by ΔP and an electroosmotic flow generated
 by E acting on 180 the charge density in the EDL given by Eq. (14).
 Consequently, the velocity 181 profile $v(r)$ in a cylindrical capillary is given
 as (Rice & Whitehead, 1965)

$$v(r) = \frac{1}{4\eta} (R^2 - r^2) \frac{\Delta P}{L_\tau} + \frac{\epsilon_r \epsilon_0 \zeta E}{\eta} \left[1 - \frac{I_0(r/\lambda)}{I_0(R/\lambda)} \right], \quad (15)$$

182 where L_τ is the length of tortuous capillaries.

183 Because the electric field E is related to the applied voltage across the 184
 porous medium ΔV by $E = \Delta V/L$ (L is the length of the porous medium as 185
 shown in Fig. 3). Eq. (15) is rewritten as

$$v(r) = \frac{1}{4\eta} (R^2 - r^2) \frac{\Delta P}{L_\tau} + \frac{\epsilon_r \epsilon_0 \zeta}{\eta} \left[1 - \frac{I_0(r/\lambda)}{I_0(R/\lambda)} \right] \frac{\Delta V}{L}. \quad (16)$$

186 The volume flow rate in the capillary is

$$q(R) = \int_0^R v(r) 2\pi r dr = \frac{\pi R^4}{8\eta} \frac{\Delta P}{L_\tau} + \frac{\pi \epsilon_r \epsilon_0 \zeta R^2}{\eta} \left[1 - \frac{2\lambda I_1(R/\lambda)}{R I_0(R/\lambda)} \right] \frac{\Delta V}{L}, \quad (17)$$

187 where I_1 is the first-order modified Bessel functions of the first kind.

188 Figure 4 shows the variation of the nondimensional parameter of the sec¹⁸⁹
 ond term in square brackets in Eq. (17) denoted by $C = 2\lambda I_1(R/\lambda)/(R I_0(R/\lambda))$
 190 with R/λ . It is seen that when the pore size is much bigger than the Debye
 191 length (hundred times), the term of $2\lambda I_1(R/\lambda)/(R I_0(R/\lambda))$ is much smaller
 192 than the unity and can be ignored (see Rice & Whitehead (1965) for more

193 details). Under that condition called the thin EDL assumption, Eq. (17) 194
 becomes

$$q(R) = \frac{\pi R^4 \Delta P}{8\eta L\tau} + \frac{\pi \epsilon_r \epsilon_0 \zeta R^2 \Delta V}{\eta L} . \quad (18)$$

195 In geological media and under most environmental conditions (i.e.,
 ground-
 196 water for human consumption or subsurface reservoirs), ionic strengths
 (i.e.,

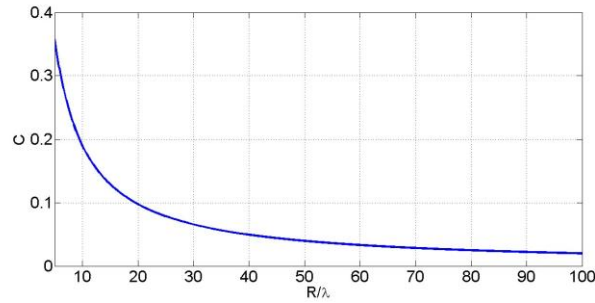


Figure 4: The variation of the unitless coefficient $C = 2\lambda_1(R/\lambda)/(Rl_0(R/\lambda))$ with the unitless ratio of the considered pore size and the Debye length (R/λ)

197 a proxy for ionic concentration) in potable water typically vary between
 198 10^{-3} and 10^{-2} mol/L (Jougnot et al., 2019). Reservoirs can be saturated
 199 with brine having much higher ionic concentrations depending on the
 for₂₀₀ formation. Therefore, the Debye length is typically less than 10 nm at
 25° C ₂₀₁ (Israelachvili, 1992). It suggests that the minimum pore radius of
 porous ma₂₀₂ terials that is applicable for thin EDL under the
 environmental conditions ₂₀₃ is around $100 \times 10 \text{ nm} = 1 \mu\text{m}$. In addition,
 typical characteristic radius of ₂₀₄ pore in geological media is tens of
 micrometer (e.g., Hu et al., 2017). There₂₀₅ fore, a thin EDL assumption
 (no EDL overlap) is normally satisfied in most ₂₀₆ natural systems (see
 Jougnot et al. (2019) for more details). It is noted that ₂₀₇ the thin EDL
 assumption does not work for clay rocks and low permeability ₂₀₈
 sediments where the pore size is on the order of 10 nm. Therefore, one
 needs ₂₀₉ to take into account the term of $C = 2\lambda_1(R/\lambda)/(Rl_0(R/\lambda))$ in Eq.
 (17). It ₂₁₀ is therefore a limitation to the proposed model.

211 *3.3. Fractal based up-scaling*

212 Porous media can be conceptualized as a bundle of tortuous capillary 213 tubes following a fractal pore-size distribution (e.g., Yu & Cheng, 2002; Liang 214 et al., 2014) (see Fig. 3). The fractal approach is a simple and elegant way to 215 upscale microscopic properties to macroscopic properties by assuming that 216 the pore size distribution follows the fractal scaling law

$$N(\geq R) = \left(\frac{R_{max}}{R}\right)^{D_f}, \quad (19)$$

217 where N is the number of capillaries with radius greater than R , R_{max} is the 218 maximum radius, D_f is the fractal dimension for pore space, $0 < D_f < 2$ 219 in two-dimensional space and $0 < D_f < 3$ in three dimensional space (Yu & 220 Cheng, 2002; Liang et al., 2014).

221 From Eq. (19), the following is obtained

$$-dN = D_f R_{max}^{D_f} R^{-D_f-1} dR, \quad (20)$$

222 where $-dN$ is the number of capillaries with radius ranging from R to $R+dR$. 223 The minus (-) in Eq. (20) implies that the number of pores decreases with 224 the increase of pore size. The total number of capillaries with radius ranging 225 from R_{min} (the minimum radius) to R_{max} (the maximum radius) is given by

$$N_{total}(\geq R_{min}) = \left(\frac{R_{max}}{R_{min}}\right)^{D_f}. \quad (21)$$

226 From Eq. (20) and Eq. (21), the following is obtained

$$-\frac{dN}{N_{total}} = D_f R_{min}^{D_f} R^{-D_f-1} dR = f(R)dR, \quad (22)$$

227 in which $f(R) = D_f R_{min}^{D_f} R^{-D_f-1}$ is the probability density function. Accord-
228 ing to the statistical theory, the probability density function needs to meet
229 the following condition

$$\int_{R_{min}}^{R_{max}} f(R)dR = 1 - \left(\frac{R_{min}}{R_{max}}\right)^{D_f} = 1 \quad (23)$$

230 **OR**

$$\left(\frac{R_{min}}{R_{max}}\right)^{D_f} \approx 0 \quad (24)$$

Eq. (24) is approximately valid for $R_{min}/R_{max} \approx 10^{-2}$ or $< 10^{-2}$ (Yu & Cheng, 2002; Liang et al., 2014). That condition generally holds in porous media. The fractal dimension D_f is linked to the porosity of porous media and the ratio of the minimum capillary radius to the maximum capillary radius ($\alpha = R_{min}/R_{max}$) by following equation (e.g., Yu et al., 2001; Yu & Cheng, 2002)

$$D_f = 2 - \frac{\ln \phi}{\ln \alpha} \quad (25)$$

3.4. REV scale

To obtain the volume flow rate at the macroscale, a representative elementary volume (REV) as a cube with a length L is considered. As presented in the previous section, the porous medium exhibits a fractal pore size distribution with radii varying from R_{min} to R_{max} . We consider the REV under varying saturation conditions. The effective saturation is defined by

$$S_e = \frac{S_w - S_{irr}}{1 - S_{irr}}, \quad (26)$$

where S_w is the water saturation and S_{irr} is irreducible water saturation. We assume that the REV is initially fully saturated and then drained when submitted to a pressure head h (m). For a capillary tube, the pore radius R_h (m) that is drained at a given pressure head h can be calculated by (Jurin, 1719)

$$h = \frac{2T_s \cos \beta}{\rho_w g R_h}, \quad (27)$$

where T_s (N/m) is the surface tension of the fluid and β is the contact angle. A capillary becomes fully desaturated under the pressure head h if R is greater than the radius R_h given by Eq. (27). Therefore, the capillaries with radii R between R_{min} and R_h will be fully saturated under the pressure head

h .

For porous media containing only large and regular pores, the irreducible water saturation can often be neglected. For porous media containing small pores, the irreducible water saturation can be pretty significant because water

remains trapped in the crevices or in micropores that are not occupied by air. ²⁵⁷This amount of water is taken into account in the model by setting irreducible ²⁵⁸water radius of capillaries R_{irr} . Consequently, the following assumptions are

²⁵⁹made in this work: (1) for $R_{min} \leq R \leq R_{irr}$, the capillaries are occupied by ²⁶⁰water that is immobile at irreducible saturation due to insufficient driving ²⁶¹force, so it does not contribute to fluid flow; (2) for $R_{irr} < R \leq R_h$, the ²⁶²capillaries are occupied by mobile water, so it contributes to the fluid flow; ²⁶³(3) for $R_h < R \leq R_{max}$, the capillaries are occupied by air, so it does not ²⁶⁴contribute to the fluid flow. In this work, film bound water adhering to ²⁶⁵the capillary walls of porous media with radius greater than R_{irr} is ignored. ²⁶⁶Therefore, the irreducible water saturation is defined as

$$S_{irr} = \frac{\int_{R_{min}}^{R_{irr}} \pi R^2 L_\tau(-dN)}{\int_{R_{min}}^{R_{max}} \pi R^2 L_\tau(-dN)} = \frac{R_{irr}^{2-D_f} - R_{min}^{2-D_f}}{R_{max}^{2-D_f} - R_{min}^{2-D_f}}. \quad (28)$$

²⁶⁷The water saturation is determined as:

$$S_w = \frac{\int_{R_{min}}^{R_h} \pi R^2 L_\tau(-dN)}{\int_{R_{min}}^{R_{max}} \pi R^2 L_\tau(-dN)} = \frac{R_h^{2-D_f} - R_{min}^{2-D_f}}{R_{max}^{2-D_f} - R_{min}^{2-D_f}}. \quad (29)$$

²⁶⁸Because only capillaries with radius between R_{min} and R_h are fully saturated ²⁶⁹under a pressure head h , the volumetric flow rate Q_{REV} through the REV ²⁷⁰is the sum of the flow rates over all capillaries with radius between R_{irr} and ²⁷¹ R_h and given by

$$Q_{REV} = \int_{R_{irr}}^{R_h} q(R)(-dN) \quad (30)$$

²⁷²Combining Eq. (18), Eq. (20) and Eq. (30), the following is obtained

$$Q_{REV} = \frac{\pi R_{max}^{D_f} D_f (R_h^{4-D_f} - R_{irr}^{4-D_f}) \Delta P}{8\eta (4-D_f) L_\tau} + \frac{\pi R_{max}^{D_f} \epsilon_r \epsilon_0 \zeta D_f (R_h^{2-D_f} - R_{irr}^{2-D_f}) \Delta V}{\eta (2-D_f) L} \quad (31)$$

²⁷³Additionally, from Eq. (28) and Eq. (29) one has

$$R_{irr} = R_{max} [\alpha^{2-D_f} + S_{irr}(1 - \alpha^{2-D_f})]^{1/(2-D_f)} \quad (32)$$

²⁷⁴and

$$R_h = R_{max} [\alpha^{2-D_f} + S_w(1 - \alpha^{2-D_f})]^{\frac{1}{2-D_f}}, \quad (33)$$

275 where $\alpha=R_{min}/R_{max}$.

276 Combining Eq. (31), Eq. (32) and Eq. (33), the following is obtained

$$Q_{REV} = \frac{\pi R_{max}^4 D_f}{8\eta(4 - D_f)} \left\{ [\alpha^{2-D_f} + S_w(1 - \alpha^{2-D_f})]^{\frac{4-D_f}{2-D_f}} - [\alpha^{2-D_f} + S_{irr}(1 - \alpha^{2-D_f})]^{\frac{4-D_f}{2-D_f}} \right\} \frac{\Delta P}{L_\tau} + \frac{\pi R_{max}^2 \epsilon_r \epsilon_0 \zeta D_f}{\eta(2 - D_f)} S_w(1 - \alpha^{2-D_f})(S_w - S_{irr}) \frac{\Delta V}{L}. \quad (34)$$

277 The total flow rate Q through the porous medium is given by

$$Q = Q_{REV} \frac{A}{A_{REV}}, \quad (35)$$

278 where A and A_{REV} are the cross sectional areas of the porous medium and
279 the REV, both are perpendicular to the flow direction.

280

281 The porosity is calculated by

$$\phi = \frac{V_{pore}}{V_{REV}} = \frac{\int_{R_{min}}^{R_{max}} L_\tau \pi R^2 (-dN)}{L A_{REV}} = \frac{\pi \tau D_f R_{max}^2 (1 - \alpha^{2-D_f})}{(2 - D_f) A_{REV}}, \quad (36)$$

282 where τ is the mean tortuosity of the porous medium defined by the
283 relation $L_\tau = \tau.L$.

284

285 The cross sectional area of the REV is therefore obtained as

$$A_{REV} = \frac{\pi \tau D_f R_{max}^2 (1 - \alpha^{2-D_f})}{(2 - D_f) \phi}. \quad (37)$$

286 Combining Eq. (34), Eq. (35) and Eq. (37), one obtains

$$Q = \frac{R_{max}^2 A (2 - D_f)}{8\eta\tau} \frac{\phi}{(4 - D_f) (1 - \alpha^{2-D_f})} \times \left\{ [\alpha^{2-D_f} + S_w(1 - \alpha^{2-D_f})]^{\frac{4-D_f}{2-D_f}} - [\alpha^{2-D_f} + S_{irr}(1 - \alpha^{2-D_f})]^{\frac{4-D_f}{2-D_f}} \right\} \frac{\Delta P}{L_\tau} + \frac{\epsilon_r \epsilon_0 \zeta \phi A}{\eta\tau} (S_w - S_{irr}) \frac{\Delta V}{L} \quad (38)$$

287 Eq. (38) indicates that the total volumetric flow rate relates to the zeta 288
potential, fluid properties (relative permittivity, viscosity), water
saturation, 289 irreducible water saturation as well as the microstructural
parameters of

290 porous media ($D_f, \phi, \alpha, r_{max}, \tau$). Eq. (38) predicts that when $S_w = S_{irr}$
291 ($S_e=0$) then $Q = 0$ (i.e., no water flow). When the porous medium is fully 292
saturated $S_w = 1$ and the irreducible water saturation equals zero $S_{irr} = 0$, 293
the total volumetric flow Q becomes

$$Q = \frac{R_{max}^2 A (2 - D_f)}{8\eta\tau} \frac{\phi}{(4 - D_f) (1 - \alpha^{2-D_f})} (1 - \alpha^{4-D_f}) \frac{\Delta P}{L\tau} + \frac{\epsilon_r \epsilon_0 \zeta \phi A \Delta V}{\eta\tau L} \quad (39)$$

294 Because $1 < D_f < 2$ and $2 < 4 - D_f < 3$, $\alpha^{4-D_f} < 1$ ($\alpha = R_{min}/R_{max} \leq$
295 10^{-2} in porous media as previously reported). Using $1 - \alpha^{2-D_f} = 1 - \phi$ as 296
shown by Eq. (25), Eq. (39) is rewritten as

$$Q = \frac{R_{max}^2 A (2 - D_f)}{8\eta\tau} \frac{\phi}{(4 - D_f) (1 - \phi)} \frac{\Delta P}{L\tau} + \frac{\epsilon_r \epsilon_0 \zeta \phi A \Delta V}{\eta\tau L} \quad (40)$$

297 Eq. (40) is exactly the same as that reported in Liang et al. (2015) under 298 the
thin EDL assumption and full saturation.

299 From Eq. (38), we will obtain the link between fluid pressure difference 300 and
flow rate as well as the electroosmotic pressure coefficient.

301 3.5. Relationship between the flow rate and back pressure difference

302 Under the condition of zero flow rate ($Q = 0$), the maximum
303 ΔP_m back pressure generated across the porous medium is obtained as

$$\Delta P_m = - \frac{8\epsilon_r \epsilon_0 \zeta \Delta V \tau (1 - \phi) (4 - D_f)}{R_{max}^2 (2 - D_f)} \times \frac{S_w - S_{irr}}{\left\{ [\alpha^{2-D_f} + S_w (1 - \alpha^{2-D_f})]^{\frac{4-D_f}{2-D_f}} - [\alpha^{2-D_f} + S_{irr} (1 - \alpha^{2-D_f})]^{\frac{4-D_f}{2-D_f}} \right\}} \quad (41)$$

304 Under the condition of zero back pressure difference ($\Delta P = 0$), the total 305 flow
rate is maximum as

$$Q_m = \frac{\epsilon_r \epsilon_0 \zeta A \phi}{\eta\tau} (S_w - S_{irr}) \frac{\Delta V}{L} \quad (42)$$

306 Combining Eq. (38), Eq. (41) and Eq. (42), the link between the pressure 307
difference and the flow rate is given by

$$Q = Q_m \left[1 - \frac{\Delta P}{\Delta P_m} \right] \quad (43)$$

308 Eq. (43) is exactly the same as that obtained in Zeng et al. (2001) in which 309
the porous medium was conceptualized as a bundle of parallel capillaries of 310
the same radii at full saturation condition. Interestingly, Eq. (43) is obtained 311
in this work for the fractal pore size distribution and for partially saturated 312
porous media but the result is the same for the relationship between flow 313
rate and pressure difference.

314 3.6. Electroosmotic pressure coefficient

315 The electroosmotic pressure coefficient K_E is defined by $\Delta P/\Delta V$, that 316 means
the K_E is a macroscopic variable (i.e., integrating over the entire 317 bundle of
capillaries) when the total flow rate Q in Eq. (38) equals zero (Li 318 et al., 1995;
Wang et al., 2016). Consequently, one has

$$K_E = \frac{\Delta P}{\Delta V} \Big|_{Q=0} = \frac{\Delta P_m}{\Delta V} \quad (44) \quad 319 \text{ Using Eq. (41), Eq. (44) is rewritten as}$$

$$K_E = - \frac{8\epsilon_r\epsilon_0\zeta\tau(1-\phi)(4-D_f)}{R_{max}^2(2-D_f)} \times \frac{S_w - S_{irr}}{\left\{ [\alpha^{2-D_f} + S_w(1-\alpha^{2-D_f})]^{\frac{4-D_f}{2-D_f}} - [\alpha^{2-D_f} + S_{irr}(1-\alpha^{2-D_f})]^{\frac{4-D_f}{2-D_f}} \right\}}. \quad (45)$$

320 Eq. (45) is a general expression for the electroosmotic pressure
coefficient

321 for partially saturated porous media. Eq. (45) indicates that the
electroos322 motic pressure coefficient is explicitly linked to ζ ,
microstructural parameters 323 of porous media (D_f , ϕ , α , R_{max} , τ), water
saturation and irreducible water 324 saturation. Therefore, the model can
indicate more mechanisms influencing 325 the electroosmotic pressure
coefficient than other published models (e.g., Eq.
326 (7) deduced by the volume averaging approach).

327 In case of full saturation $S_w = 1$, Eq. (45) becomes

$$K_E^{sat} = - \frac{8\epsilon_r\epsilon_0\zeta\tau(1-\phi)(4-D_f)}{R_{max}^2(2-D_f)} \frac{1-S_{irr}}{\left\{1 - [\alpha^{2-D_f} + S_{irr}(1-\alpha^{2-D_f})]^{\frac{4-D_f}{2-D_f}}\right\}}. \quad (46)$$

328 The relative electroosmotic pressure coefficient K_E^r is defined as

$$\begin{aligned} K_E^r &= \frac{K_E}{K_E^{sat}} = \frac{S_w - S_{irr}}{1 - S_{irr}} \frac{\left\{1 - [\alpha^{2-D_f} + S_{irr}(1-\alpha^{2-D_f})]^{\frac{4-D_f}{2-D_f}}\right\}}{\left\{[\alpha^{2-D_f} + S_w(1-\alpha^{2-D_f})]^{\frac{4-D_f}{2-D_f}} - [\alpha^{2-D_f} + S_{irr}(1-\alpha^{2-D_f})]^{\frac{4-D_f}{2-D_f}}\right\}} \\ &= S_e \frac{\left\{1 - [\alpha^{2-D_f} + S_{irr}(1-\alpha^{2-D_f})]^{\frac{4-D_f}{2-D_f}}\right\}}{\left\{[\alpha^{2-D_f} + S_w(1-\alpha^{2-D_f})]^{\frac{4-D_f}{2-D_f}} - [\alpha^{2-D_f} + S_{irr}(1-\alpha^{2-D_f})]^{\frac{4-D_f}{2-D_f}}\right\}}. \end{aligned} \quad (47)$$

329 4. Results and discussion

330 4.1. Predictions of the model under partially saturated conditions

331 The values of α between 0.001 and 0.01 are used in this section for model³³²
ing because those values are normally used in published works (Yu & Cheng, ³³³
2002; Liang et al., 2014; Thanh et al., 2019). The fractal dimension D_f is in ³³⁴the
range between 1 and 2. For given porous media, D_f is determined via ³³⁵Eq. (25)
with known values of α and porosity ϕ . Fig. 5 shows (a) the influ³³⁶ence of the
irreducible saturation on the change of the relative electroosmotic ³³⁷pressure
coefficient K_E^r with the water saturation S_w ($S_{irr} = 0.02, 0.05$ and

338 0.1) for $\alpha = 0.01$ and $D_f = 1.8$; (b) influence of α on the variation of K_E^r

339 with S_w ($\alpha = 0.002, 0.005, 0.01$) for $S_{irr} = 0.05$ and $D_f = 1.8$ and (c) Influ³⁴⁰ence
of D_f on the variation of K_E^r with S_w ($D_f = 1.3, 1.5, 1.8$) for $\alpha = 0.01$ ³⁴¹and $S_{irr} =$
0.05. The results show that as the media desaturate, the relative ³⁴²
electroosmotic pressure coefficient K_E^r increases. The reason is that at lower
³⁴³water saturation, only capillaries with smaller radii are occupied by
water. ³⁴⁴Therefore, one needs larger pressure differences over porous
media to counter ³⁴⁵balance with the flow rate generated by the same
applied voltage (such that ³⁴⁶the total volumetric flow rate is zero). As a
result, K_E^r is larger for lower

347 water saturation. Additionally, Fig. 5 shows that the relative electroosmotic 348
 pressure coefficient is very sensitive to the fractal dimension D_f and the ratio 349
 α . It is noted that the D_f decreases with an increase of α at a given porosity 350 as
 indicated by Eq. (25). Fig. 5 also shows that the K_E^r decreases with the 351
 increase of the ratio α and decrease of D_f . That can be explained by the 352
 decrease of the total number of pores in the REV with the decrease of D_f .

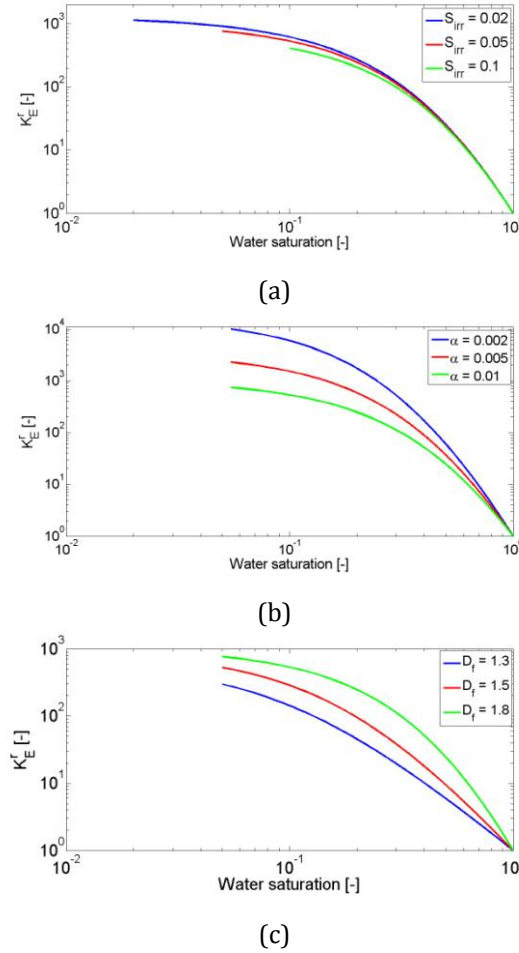


Figure 5: Sensitivity analysis of the model: (a) Influence of the irreducible saturation on the variation of the K_E^r with the water saturation S_w ($S_{irr} = 0.02, 0.05$ and 0.1) for $\alpha = 0.01$ and $D_f = 1.8$; (b) Influence of α on the variation of K_E^r with S_w ($\alpha = 0.002, 0.005, 0.01$) for $S_{irr} = 0.05$ and $D_f = 1.8$; (c) Influence of D_f on the variation of K_E^r with S_w ($D_f = 1.3, 1.5, 1.8$) for $\alpha = 0.01$ and $S_{irr} = 0.05$.

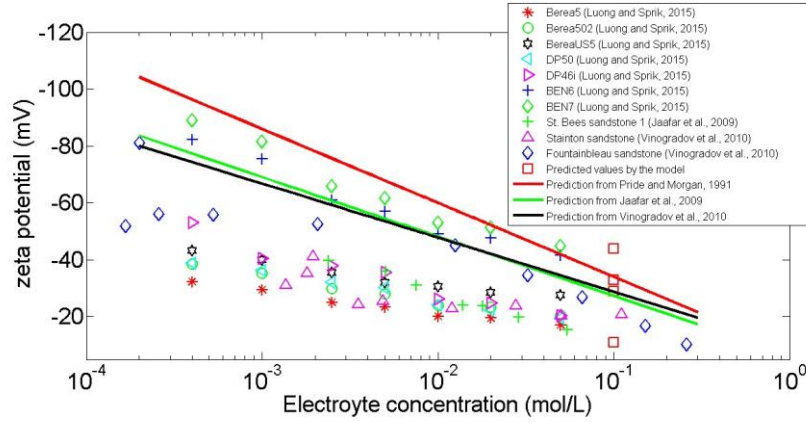


Figure 6: The variation of the zeta potential with pore fluid salinity. The predicted values of the zeta potential for four samples of glass beads at 0.1 mol/L in Li et al. (1995) are shown by red squares. Experimental data from different sources reported by Thanh & Sprik (2015), Jaafar et al. (2009) and Vinogradov et al. (2010) are also presented.

353 Therefore, R_h becomes larger at the same water water saturation. Similarly, 354
 we need to apply a smaller pressure difference over the partially saturated 355
 REV to counter balance the flow rate generated by the same applied voltage. 356
 Consequently, K_E^r decreases with a decrease of D_f .

357 4.2. Comparison with experimental data in water saturated porous media

358 Even if the present model is developed based on the concept of capillary 359
 tubes, it possible to provide a relationship between capillary radius to grain 360
 size for the sake of medium characterization. Indeed, in non-consolidated 361
 granular materials, pore size are very difficult to obtain without perturbat-
 362 ing the medium, while grain sizes and grain size distribution can be easily 363
 measured. Therefore, with the knowledge of the mean grain diameter d of 364 a
 granular material, the maximum pore radius can be determined by (e.g., 365 Liang
 et al., 2015)

$$R_{max} = \frac{d}{4} \left[\sqrt{\frac{\phi}{1-\phi}} + \sqrt{\frac{1}{1-\phi}} \right]. \quad (48)$$

366 Mean geometrical tortuosity of porous media is predicted from porosity 367 as
 (e.g., Cai et al., 2012a; Ghanbarian et al., 2013; Liang et al., 2015)

$$\tau = \frac{1}{2} \left[1 + \frac{1}{2} \sqrt{1-\phi} + \sqrt{1-\phi} \frac{\sqrt{(1/\sqrt{1-\phi} - 1)^2 + 1/4}}{1 - \sqrt{1-\phi}} \right] \quad (49)$$

Table 1: Input parameters of four samples of fused glass beads are taken from Li et al. (1995). Symbols of d , φ , K_E and α are symbols for the grain diameter, porosity, the electroosmotic pressure coefficient and ratio of minimum and maximum radius, respectively. The values of ζ are predicted from Eq. (45)

Number	d (μm)	φ (no units)	K_E (Pa/V)	α (no units)	ζ (mV)
1	50	0.10	4.94	0.01	-11
2	50	0.17	12.5	0.01	-48
3	100	0.19	1.9	0.01	-33
4	200	0.30	0.25	0.01	-29
mean					-30

³⁶⁸ We want to see if the model is able to predict the zeta potential using Eq. ³⁶⁹ (46). Li et al. (1995) measured K_E for fused glass beads fully saturated by ³⁷⁰ a 0.1 M NaCl electrolyte. Micro-structure parameters of the samples such ³⁷¹ as grain diameter d , porosity φ as well as the measured K_E are reported in ³⁷² Li et al. (1995) and re-shown in Table 1. At this electrolyte concentration, ³⁷³ the Debye length λ is around 1 nm (Israelachvili, 1992). Of all samples, ³⁷⁴ the minimum value of R_{max} corresponding to the sample 1 ($d=50 \mu\text{m}$ and ³⁷⁵ $\varphi=0.1$) is predicted using Eq. (48) to be 17 μm . Hence, R_{min} corresponding

³⁷⁶ to the sample 1 is obtained using $R_{min} = \alpha R_{max} = 0.01 R_{max} = 170 \text{ nm}$. ³⁷⁷ Consequently, the Debye length is much smaller than R_{min} and Eq. (46) is ³⁷⁸ applicable for experimental data reported by Li et al. (1995).

³⁷⁹ The value of α is taken as 0.01 because that is a normally used value ³⁸⁰ for grain materials (e.g., Thanh et al., 2018, 2019). The value of S_{irr} is ³⁸¹ reasonably taken as 0 for large grain materials (e.g., Jougnot et al., 2012). ³⁸² From the known values of porosity φ and α of samples (see Table 1), D_f is ³⁸³ obtained by Eq. (25). From Eq. (46), the zeta potential is obtained with the ³⁸⁴ knowledge of α , D_f , τ , φ , R_{max} and S_{irr} . The predicted values are presented ³⁸⁵ in Table 1. It is seen that the predicted values (see red squares at 0.1 mol/L ³⁸⁶ in Fig. 6) are in good agreement with published experimental data (Jaafar ³⁸⁷ et al., 2009; Vinogradov et al., 2010; Thanh & Sprik, 2015).

³⁸⁸ The zeta potential is dependent on the electrical conductivity of the fluid. ³⁸⁹ The electroosmotic pressure coefficient K_E^{sat} varies with the electrolyte elec³⁹⁰ trical conductivity σ_w . Fig. 7 shows the variation of the electroosmotic pres³⁹¹ sure coefficient with fluid electrical conductivity experimentally obtained by

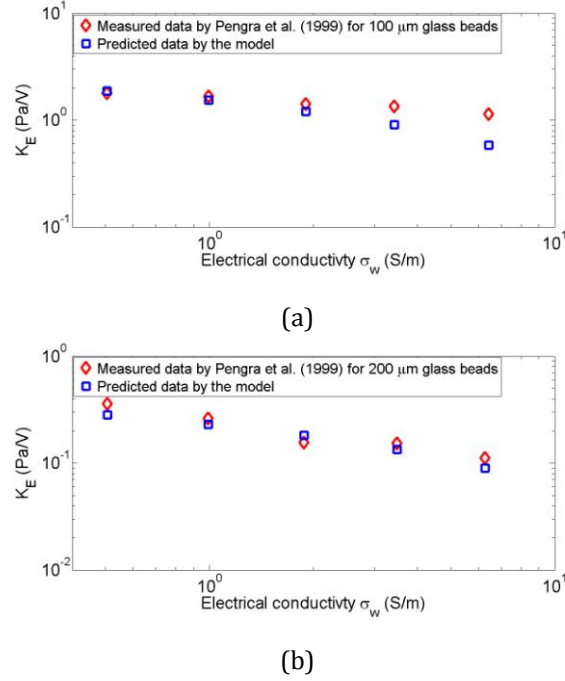


Figure 7: Variation of the electroosmotic pressure coefficient K_E^{sat} at saturated condition with electrolyte electrical conductivity for two consolidated samples of glass beads: (a) for the sample of 100 μm glass beads and (b) for the sample of 200 μm glass beads shown in Table 1).

392 Pengra et al. (1999) for two samples of glass beads ($d=100\ \mu\text{m}$ and $200\ \mu\text{m}$, 393 respectively) saturated by a NaCl electrolyte (see diamond symbols). There 394 are few proposed expressions for the relationship between the zeta potential 395 and electrolyte concentration available in the literature (e.g., Pride & Moran, 1991; Jaafar et al., 2009; Vinogradov et al., 2010). One is given by $\zeta = 397 a + b \log_{10}(C_f)$ with $a = -6.43\ \text{mV}$, $b = 20.85\ \text{mV}$ as shown by Jaafar et al. 398 (2009), for example. Electrical conductivity of the NaCl electrolyte is linked 399 to the electrolyte concentration by the relation $\sigma_w = 10C_f$ for the ranges 400 $10^{-6}\text{M} < C_f < 1\ \text{M}$ and $15^\circ\text{C} < T < 25^\circ\text{C}$ (Sen & Goode, 1992). Therefore, 401 the relation $\zeta = -6.43 + 20.85 \log_{10}(0.1\sigma_w)$ (mV) is obtained. Similarly, we 402 obtain $R_{min} = 400\ \text{nm}$ for two samples and maximum value of $\lambda = 1.36\ \text{nm}$ 403 for the considered range of electrolyte concentration by Pengra et al. (1999) 404 (from $0.05\ \text{mol/L}$ to $0.65\ \text{mol/L}$). Therefore, the thin EDL assumption is 405 satisfied. Applying the same approach as we did previously, the variation 406 of the electroosmotic pressure coefficient K_E^{sat} with electrical conductivity 407 σ_w is predicted as shown in Fig. 7 by square symbols. One can see that 408 the model prediction is also in

good match with data measured by Pengra ⁴⁰⁹ et al. (1999) (diamond symbols) even there is a large difference between the ⁴¹⁰ model prediction and measured data for smaller glass beads at high electrical ⁴¹¹ conductivity. The reason may be that Jaafar et al. (2009) obtained:

$$\zeta = a + b \log_{10}(C_f) \quad (50)$$

⁴¹² by fitting experimental data for quartz, silica, glass and St. Bees in NaCl ⁴¹³ brine with big data scattering. As shown in Fig. 3 of Jaafar et al. (2009),

⁴¹⁴ the difference in ζ can reach 65% at $C_f = 10^{-2}$ mol/L. Therefore, the $\zeta - C_f$
⁴¹⁵ relation may not work well for a single silica-based sample in a large range
⁴¹⁶ of electrolyte concentration. As a matter of fact, Cherubini et al. (2018) ⁴¹⁷
show that, for data on carbonate materials, the best fit they obtain is rather
⁴¹⁸ $a = -6.97$ mV and $b = 9.13$ mV, indicating that this relationship is largely ⁴¹⁹
mineral dependent.

⁴²⁰ Figure 8 shows the variation of ΔP_m with an applied voltage for the 10 ⁴²¹ μm
sand pack saturated with 10^{-3} M NaCl. The symbols are deduced from ⁴²² Luong
& Sprik (2013) (their Fig. 10) using the relation $\Delta P_m = \rho g \Delta h_m$ (Δh_m

⁴²³ is the maximum height difference obtained from Luong & Sprik (2013), ρ
=
⁴²⁴ 1000 kg/m³ is the water density and $g = 10$ m/s² is the acceleration due
to

Table 2: Parameters taken from Wang et al. (2015) for 10 sandstone samples in which ϕ , k , ζ stand for porosity, permeability, the zeta potential. The electroosmotic pressure coefficient K_E^{exp} is deduced by comparison between the similarity of porosity, permeability, depth of samples between Wang et al. (2015) and Wang et al. (2016). K_E^{theo} is predicted from the model.

Sample	ϕ (no units)	k (10 ⁻¹⁵ m ²)	ζ (V)	K_{Eexp} (Pa/V)	K_{Etheo} (Pa/V)
D1	30.6	1028	-0.0486	0.42	0.44
D2	30.2	1435	-0.0571	0.47	0.35
D3	30.9	1307	-0.0410	0.40	0.31
D4	32.1	1152	-0.0609	0.40	0.61
D5	29.8	456	-0.0727	0.52	1.30
D6	31.0	978	-0.0462	0.51	0.46
D7	29.4	594	-0.0627	0.49	0.82
D8	31.0	2785	-0.1448	0.52	0.51
D9	29.3	1491	-0.0765	0.43	0.40

D10 31.5 3241 -0.0639 0.51 0.21

425 gravity). At the saturated condition, Eq. (41) becomes

$$\Delta P_m = - \frac{8\epsilon_r\epsilon_0\zeta\Delta V\tau(1-\phi)(4-D_f)}{R_{max}^2(2-D_f)} \times \frac{1-S_{irr}}{\left\{1 - [\alpha^{2-D_f} + S_{irr}(1-\alpha^{2-D_f})]^{\frac{4-D_f}{2-D_f}}\right\}} \quad (51)$$

426 The solid line is predicted from Eq. (51) in the same manner as mentioned 427 above with $\phi = 0.38$, $D_f = 0.01$, $d = 10 \mu\text{m}$, $\alpha = 0.01$ and the mean value

428 of $\zeta = -13 \text{ mV}$ over six granular samples made of spherical grains (Luong & 429 Sprik, 2013) (best fit is obtained with $S_{irr} = 0$). Note that the thin EDL is not 430 really met in this case because of $R_{min} \approx 60 \text{ nm}$ and $\lambda = 9.6 \text{ nm}$. Therefore, 431 the model may not work really well to reproduce the experimental data as

432 shown in Fig. 8.

433 Eq. (46) is applied to determine the electroosmotic pressure
434 K_E coefficient for ten sandstone samples (20 mm in length and 25 mm in diameter) sat435 urated by a 0.05 M NaCl electrolyte reported in Wang et al. (2015). Parame436 ters of the sandstone samples and the measured zeta potential are presented

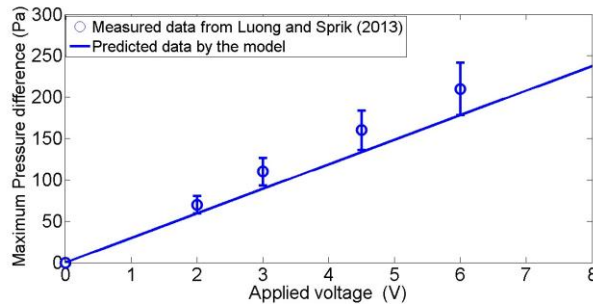


Figure 8: Maximum pressure difference as a function of applied voltage. The symbols are experimental data from Luong & Sprik (2013) with $\pm 15\%$ of uncertainty and the solid line is obtained from Eq. (51)

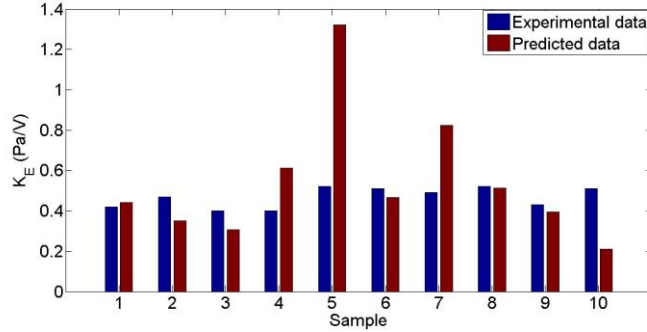


Figure 9: The variation of the K_E predicted in this work and the experimental data taken from Wang et al. (2015)

437 by Wang et al. (2015) and re-shown in Table 2. The measured values of K_E ⁴³⁸ are obtained by the same research group Wang et al. (2016) for the same
 439 conditions and re-presented in Table 2 (see K_E ^{exp}). To estimate the mean⁴⁴⁰ grain diameter of porous media from the permeability, we use the relation
 441 given by (e.g., Bernabe & Revil, 1995; Revil et al., 1999; Glover et al., 2006)

$$d = \sqrt{\frac{4am^2k}{\phi^{3m}}} \quad (52)$$

442 where the cementation exponent m is taken as 1.9 for consolidated sandstone⁴⁴³ (Friedman, 2005) and a is a constant between 2-12 that depends on the pore⁴⁴⁴ space (Glover et al., 2006; Glover & Walker, 2009). In this part, a is taken⁴⁴⁵ as 4 for a set of samples of Wang et al. (2015). With estimated values of⁴⁴⁶ d , measured ϕ and $\alpha = 0.001$ (that value is also relevant to that used in⁴⁴⁷ Liang et al. (2014) for a Fontainebleau sandstone), the K_E is predicted for⁴⁴⁸ reported in Table 2 (K_E^{theo}). Fig. 9 shows the predicted K_E calculated in⁴⁴⁹ this work and measured values taken from Wang et al. (2015). It is seen that⁴⁵⁰ Eq. (46) predicts the published experimental data well. Note that for this⁴⁵¹ set of experimental data, we obtain the minimum value of $R_{min} \approx 2.10^3$ nm⁴⁵² and $\lambda = 1.36$ nm. Therefore, the thin EDL assumption is satisfied and Eq.⁴⁵³ (46) is valid.

454 4.3. Prediction of the product of the permeability and formation factor

455 Comparing Eq. (7) and Eq. (46), the product of the permeability and⁴⁵⁶ formation factor of porous media is given by

$$kF = \frac{R_{max}^2(2 - D_f)}{8\tau(1 - \phi)(4 - D_f)} \frac{\left\{ 1 - [\alpha^{2-D_f} + S_{irr}(1 - \alpha^{2-D_f})]^{\frac{4-D_f}{2-D_f}} \right\}}{1 - S_{irr}} \quad (53)$$

Eq. (53) indicates that based on the fractal model for electroosmotic flow in porous media, one can get the product of the permeability and formation factor from the parameters D_f , R_{max} , τ , α and S_{irr} of porous media. Eq. (53) is now used to estimate the product of kF and compare with experimental data reported in Glover et al. (2006), Glover & D'ery (2010) and Bolève et al. (2007) for 27 samples of bead packs. Parameters for the samples (grain diameter, porosity, permeability) are taken from Glover et al. (2006), Glover & D'ery (2010) and Bolève et al. (2007) and re-shown in Table 3. The values

Table 3: Input parameters for bead packs taken from Glover et al. (2006), Glover & D'ery (2010) and Bolève et al. (2007). Symbols of d (μm), ϕ (no units), k (m^2), F (no units) and α (no units) stand for grain diameter, porosity, permeability, formation factor and ratio of minimum and maximum radius, respectively.

No.	d (μm)	ϕ (-)	k (10^{-12} m^2)	F (-)	α (-)	reference
1	20	0.40	0.2411	3.90	0.01	Glover et al. (2006)
2	45	0.39	1.599	4.01	0.01	Glover et al. (2006)
3	106	0.39	8.118	4.04	0.01	Glover et al. (2006)
4	250	0.40	50.46	3.97	0.01	Glover et al. (2006)
5	500	0.38	186.79	4.08	0.01	Glover et al. (2006)
6	1000	0.40	709.85	3.91	0.01	Glover et al. (2006)
7	2000	0.39	2277.26	4.13	0.01	Glover et al. (2006)
8	3350	0.40	7706.97	3.93	0.01	Glover et al. (2006)
9	1.05	0.411	0.00057	3.80	0.01	Glover & D'ery (2010)
10	2.11	0.398	0.00345	3.98	0.01	Glover & D'ery (2010)
11	5.01	0.380	0.0181	4.27	0.01	Glover & D'ery (2010)
12	11.2	0.401	0.0361	3.94	0.01	Glover & D'ery (2010)
13	21.5	0.383	0.228	4.22	0.01	Glover & D'ery (2010)
14	31	0.392	0.895	4.07	0.01	Glover & D'ery (2010)
15	47.5	0.403	1.258	3.91	0.01	Glover & D'ery (2010)
16	104	0.394	6.028	4.04	0.01	Glover & D'ery (2010)
17	181	0.396	21.53	4.01	0.01	Glover & D'ery (2010)
18	252	0.414	40.19	3.75	0.01	Glover & D'ery (2010)
19	494	0.379	224	4.29	0.01	Glover & D'ery (2010)
20	990	0.385	866.7	4.19	0.01	Glover & D'ery (2010)

21	56	0.4	2.0	3.3	0.01	Bol`eve et al. (2007)
22	72	0.4	3.1	3.2	0.01	Bol`eve et al. (2007)
23	93	0.4	4.4	3.4	0.01	Bol`eve et al. (2007)
24	181	0.4	27	3.3	0.01	Bol`eve et al. (2007)
25	256	0.4	56	3.4	0.01	Bol`eve et al. (2007)
26	512	0.4	120	3.4	0.01	Bol`eve et al. (2007)
27	3000	0.4	14000	3.6	0.01	Bol`eve et al. (2007)

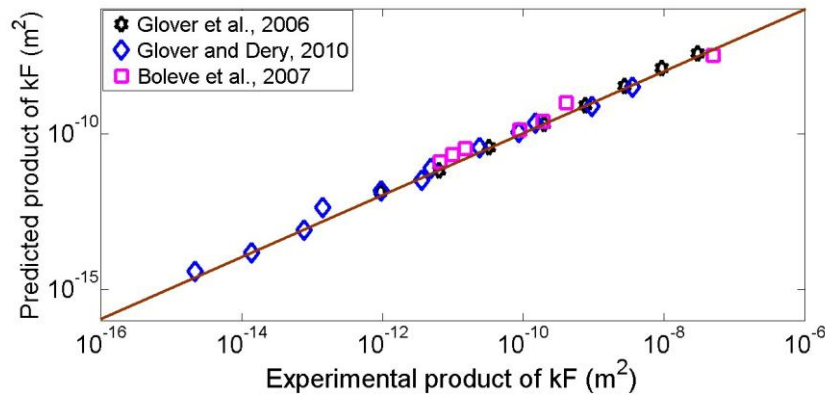


Figure 10: A comparison between kF predicted from Eq. (53) and from measured data in Glover et al. (2006), Glover & D`ery (2010) and Bol`eve et al. (2007) (the solid line is a 1:1 line).

465 of α and S_{irr} are taken as 0.01 and 0, respectively. Value of τ is obtained by 466
the relation $\tau = \varphi F$. From those parameters in combination with Eq. (53), 467
the product of the permeability and formation factor is predicted in the same 468
procedure as previously mentioned. Fig. 10 shows the comparison between
469 the product of kF predicted in this work and the experimental data. The 470
solid line represents a 1:1 line. It is seen that the predicted values are in very 471
good match with the experimental data. It suggests that one can predict k 472 of
porous materials from Eq. (53) with the knowledge of F and vice versa.

473 4.4. Electrokinetic coupling under partially saturated condition

474 Based on Eq. (3) and Eq. (5), the relationship between the electroosmosis 475
coefficient and the streaming potential coefficient is obtained as

$$K_S(S_w) = \frac{K_E(S_w)k(S_w)}{\sigma(S_w)\eta} \quad (54)$$

476 Therefore, the relative streaming potential coefficient is given as

$$K_S^r = \frac{K_S(S_w)}{K_S^{sat}(S_w = 1)} = \frac{K_E(S_w)}{K_E^{sat}(S_w = 1)} \frac{k(S_w)}{k(S_w = 1)} \frac{\sigma(S_w = 1)}{\sigma(S_w)}, \quad (55)$$

477 where $K_E^r = \frac{K_E(S_w)}{K_E^{sat}(S_w=1)}$ is given in Eq. (47), $\frac{k(S_w)}{k(S_w=1)}$ and $\frac{\sigma(S_w)}{\sigma(S_w=1)}$ are called
 478 the relative permeability and the relative conductivity of porous media and
 479 denoted by k^r and σ^r , respectively. In this work, we do not have
 expressions 480 for k^r and σ^r based on the fractal theory yet. Therefore, we use
 expressions 481 given by (e.g., Revil et al., 2007; Linde et al., 2006) for k^r and
 σ^r :

$$k^r = S_e^{(2+3\lambda)/\lambda} \quad (56)$$

482 and

$$\sigma^r = S_w^n, \quad (57)$$

483 where λ is the curve-shape parameter and n is the
 saturation exponent. 484 Eq. (57) is valid for the negligible
 surface conductivity.

485 Combining Eq. (47), Eq. (55), Eq. (56) and Eq. (57), the
 relative

486 streaming potential coefficient is given by

$$K_S^r = S_e \frac{\left\{ 1 - [\alpha^{2-D_f} + S_{irr}(1 - \alpha^{2-D_f})]^{\frac{4-D_f}{2-D_f}} \right\}}{\left\{ [\alpha^{2-D_f} + S_w(1 - \alpha^{2-D_f})]^{\frac{4-D_f}{2-D_f}} - [\alpha^{2-D_f} + S_{irr}(1 - \alpha^{2-D_f})]^{\frac{4-D_f}{2-D_f}} \right\}} \times S_e^{(2+3\lambda)/\lambda} \frac{1}{S_w^n}. \quad (58)$$

487 Additionally, Revil et al. (2007) used the volume averaging approach to
 get 488 the relative streaming potential coefficient as

$$K_S^r = S_e^{(2+3\lambda)/\lambda} \frac{1}{S_w^{n+1}}. \quad (59)$$

489 Figure 11 shows the change of the relative streaming potential coefficient
 490 K_S^r with the water saturation predicted from Eq. (58) and Eq. (59). Input 491
 parameters for modeling in Fig. 11 are $n=2.7$, $\lambda=0.87$, $S_{irr}=0.36$ which 492 are

reported by Revil et al. (2007), $D_f=1.5$ and $\alpha=0.01$ which are used due to the best fit. Additionally, a comparison between those models and experimental data reported in Revil et al. (2007) for the dolomite sample E3 (square symbols) is also shown in Fig. 11. A good agreement is observed between the proposed model, the model presented by Revil et al. (2007) and experimental data. Clearly, both theoretical models are able to describe the decrease of the relative streaming potential coefficient with decreasing water saturation, from full saturation to nearly irreducible water saturation as indicated by experimental data. When S_w decreases then the number of

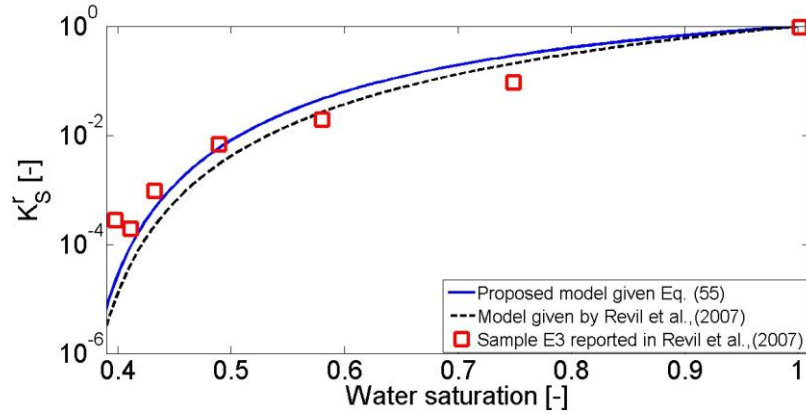


Figure 11: Variation of the coefficient K_S^r with the water saturation ($n=2.7$, $\lambda=0.87$, $S_{irr}=0.36$, $D_f=1.5$ and $\alpha=0.01$). The solid and dashed lines correspond to the proposed model (see Eq. (58)) and the model of Revil et al. (2007), respectively.

capillaries occupied by water in the REV decreases. Hence, the streaming current through the REV generated by a fluid flow becomes smaller at a given fluid pressure difference. Consequently, the K_S^r decreases with decreasing S_w as predicted.

4.5. Effective excess charge density

From Eq. (3), Eq. (4), Eq. (5) and Eq. (46), the effective excess charge density \hat{Q}_v (C/m³) under fully saturated conditions is deduced as

$$\hat{Q}_v = \frac{8\epsilon_r\epsilon_0\zeta\tau(1-\phi)(4-D_f)}{R_{max}^2(2-D_f)} \frac{1-S_{irr}}{\left\{1 - [\alpha^{2-D_f} + S_{irr}(1-\alpha^{2-D_f})]^{\frac{4-D_f}{2-D_f}}\right\}} \quad (60)$$

When one neglects the irreducible water saturation, Eq. (60) reduces to

$$\hat{Q}_v = \frac{8\epsilon_r\epsilon_0\zeta\tau(1-\phi)(4-D_f)}{R_{max}^2(2-D_f)} \quad (61)$$

509

510 Based on Eq. (61), we can calculate \hat{Q}_v for the glass beads reported 511 in
 Glover & D'ery (2010) and Bol'ev'e et al. (2007) using the same approach 512
 mentioned above. The values of the zeta potential are reported to be $\zeta =$ 513 -
 24.72 mV and -73.34 mV in Glover & D'ery (2010) and $\zeta =$ -17.5 mV, -44.7

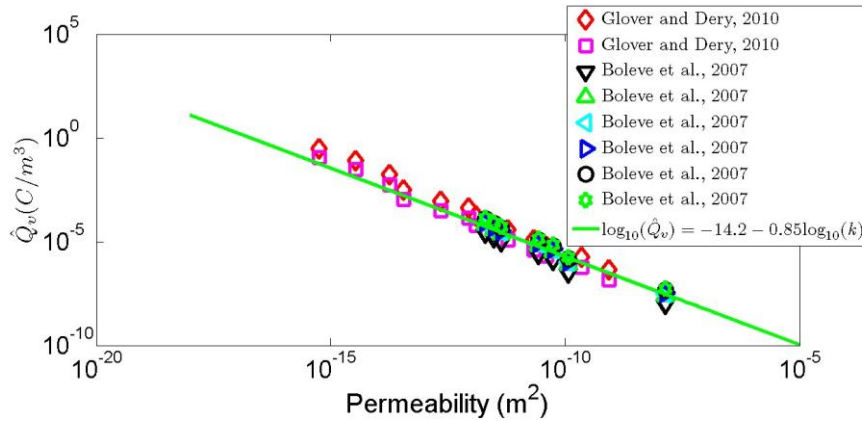


Figure 12: Variation of the effective excess charge density Q_{bv} with the permeability k . Symbols represent experimental data from Glover & D'ery (2010) and Bol'ev'e et al. (2007) (Table 3). The solid line is the fit line with $\log_{10}(\hat{Q}_v) = -14.2 - 0.85\log_{10}(k)$.

514 mV, -54.6 mV, -59.7 mV, -87.9 mV and -99.3 mV in Bol'ev'e et al. (2007)
 515 (see their Fig. 8). From calculated \hat{Q}_v , we can plot the $\hat{Q}_v - k$ graph (in 516
 which k is taken from Table 3) as shown in Fig. 12 from which we obtain

517 the fit line: $\log_{10}(Q_{bv}) = A_1 + A_2\log_{10}(k)$ with $A_1 = -14.2$ and $A_2 = -0.85$. 518 The
 obtained $Q_{bv} - k$ relationship is in good agreement with that reported

519 by Jardani et al. (2007) by fitting to a large set of experimental data that
 520 includes various lithologies and ionic concentrations: $\log_{10}(\hat{Q}_v) = -9.23 - 0.82$
 521 $\log_{10}(k)$. The constant $A_2 = -0.85$ obtained in this work is related to rock 522
 properties (R_{max} , α , τ , ϕ and D_f) and is very close to -0.82 reported by 523
 Jardani et al. (2007). The obtained constant $A_1 = -14.2$ deviates largely 524
 from value of -9.23 proposed by Jardani et al. (2007). The reason is that 525
 A_1 is mainly dependent of chemical and interface parameters (Guarracino 526

& Jougnot, 2018). Therefore, it varies with mineral composition of rocks, electrolyte concentration, types of electrolyte etc.

5. Conclusions

We derive a physically based model for electroosmotic flow in porous media in which the minimum pore radius is 100 times the Debye length that is around 1 μm under environmental conditions. The porous medium is conceptualized as a bundle of tortuous capillary tubes with a pore-size distribution following a fractal law. The obtained model is linked to the applied voltage, back pressure, water saturation, irreducible water saturation and microstructural parameters of porous materials $(D_f, \phi, \alpha, r_{max}, \tau)$. From the model, the expressions for the electroosmosis pressure coefficient, the relative electroosmosis pressure coefficient, the maximum back pressure, the maximum flow rate, the flow rate-applied back pressure relation and the product of the permeability and formation factor of porous media are also obtained. To validate the model, the sensitivity of the relative electroosmosis pressure coefficient K_E^r to S_{irr} , α and D_f is analyzed and explained. The model predictions are then compared with published data in both cases of full saturation and partial saturation. The comparisons show that our model is able to explain well experimental data. From K_E^r , the expression for the relative streaming potential coefficient K_S^r is also deduced. From that, the variation of K_S^r with the water saturation is predicted and compared with another model as well as experimental data from the dolomite rock sample. Additionally, we also obtain an expression for the effective excess charge density \hat{Q}_v . We find a good agreement between those obtained expressions and published data. We believe that the model proposed in this study can open up to new studies and modelling regarding electroosmotic phenomena and paving the way to the development of new applications and technical development in various disciplines from contaminated porous media remediation to masonry structures dewatering.

Acknowledgments

This research is funded by Vietnam National Foundation for Science and Technology Development (NAFOSTED) under grant number 103.99/2019.316. Additionally, D. Jougnot and A. Mendieta strongly thank the

financial support of ANR EXCITING (grant ANR-17-CE06-0012) for the ⁵⁶⁰ PhD thesis funding of A. Mendieta.

⁵⁶¹ **References**

⁵⁶² Bandopadhyay, A., DasGupta, D., Mitra, S. K., & Chakraborty, S. (2013). ⁵⁶³ Electro-osmotic flows through topographically complicated porous media: ⁵⁶⁴ Role of electropermeability tensor. *Phys. Rev. E*, *87*, 033006.

⁵⁶⁵ Bernabe, Y., & Revil, A. (1995). Pore-scale heterogeneity, energy dissipation ⁵⁶⁶ and the transport properties of rocks. *Geophysical Research Letters*, *22*, ⁵⁶⁷ 1529–1532.

⁵⁶⁸ Bertolini, L., Coppola, L., Gastaldi, M., & Redaelli, E. (2009). Electroos⁵⁶⁹ motic transport in porous construction materials and dehumidification of ⁵⁷⁰ masonry. *Construction and Building Materials*, *23*, 254 – 263.

⁵⁷¹ Bol`eve, A., Crespy, A., Revil, A., Janod, F., & Mattiuzzo, J. L. (2007). ⁵⁷² Streaming potentials of granular media: Influence of the dukhin and ⁵⁷³ reynolds numbers. *Journal of Geophysical Research*, *B08204*.

⁵⁷⁴ Bruell, C. J., Segall, B. A., & Walsh, M. T. (1992). Electroosomotic removal ⁵⁷⁵ of gasoline hydrocarbons and tce from clay. *Journal of Environmental* ⁵⁷⁶ *Engineering*, *118*, 68–83.

⁵⁷⁷ Bruus, H. (2008). *Theoretical Microfluidics*. Oxford University Press; ⁵⁷⁸ 1 edition.

⁵⁷⁹ Cai, J. C., Hu, X. Y., Standnes, D. C., & You, L. J. (2012a). An analytical ⁵⁸⁰ model for spontaneous imbibition in fractal porous media including gravity. ⁵⁸¹ *Colloids and Surfaces, A: Physicocemical and Engineering Aspects*, *414*, ⁵⁸² 228–
233.

⁵⁸³ Cai, J. C., You, L. J., Hu, X. Y., Wang, J., & Peng, R. H. (2012b). Pre⁵⁸⁴ diction of effective permeability in porous media based on spontaneous ⁵⁸⁵ imbibition effect. *International Journal of Modern Physics C*, *23*, DOI: ⁵⁸⁶ 10.1142/S0129183112500544.

⁵⁸⁷ Casagrande, L. (1983). Stabilization of soils by means of electroosmotic ⁵⁸⁸ state-of-art. *Journal of Boston Society of Civil Engineering, ASCE*, *69*, ⁵⁸⁹ 255–302.

- 590 Cherubini, A., Garcia, B., Cerepi, A., & Revil, A. (2018). Streaming potential coupling coefficient and transport properties of unsaturated carbonate rocks. *Vadose Zone Journal*, 17, 180030.
- 593 Davis, J., James, R., & Leckie, J. (1978). Surface ionization and complexation at the oxide/water interface. i. computation of electrical double layer properties in simple electrolytes. *Journal of Colloid and Interface Science*, 63.
- 597 Feder, J., & Aharony, A. (1989). *Fractals in Physics*. North Holland, Amsterdam.
- 599 Friedman, S. P. (2005). Soil properties influencing apparent electrical conductivity: a review. *Computers and Electronics in Agriculture*, 46, 45 – 70.
- 602 Ghanbarian, B., Hunt, A., P. Ewing, R., & Sahimi, M. (2013). Tortuosity in porous media: A critical review. *Soil Science Society of America Journal*, 77, 1461–1477.
- 605 Gierst, L. (1966). Double layer and electrode kinetics. *Journal of the American Chemical Society*, 88, 4768–4768.
- 607 Glover, P., I. Zadjali, I., & A Frew, K. (2006). Permeability prediction from micp and nmr data using an electrokinetic approach. *Geophysics*, 71, F49–F60.
- 610 Glover, P. W. J., & D'ery, N. (2010). Streaming potential coupling coefficient of quartz glass bead packs: Dependence on grain diameter, pore size, and pore throat radius. *Geophysics*, 75, F225–F241.
- 613 Glover, P. W. J., & Walker, E. (2009). Grain-size to effective pore-size transformation derived from electrokinetic theory. *Geophysics*, 74(1), E17–E29.
- 616 Good, B. T., Bowman, C. N., & Davis, R. H. (2006). An effervescent reaction micropump for portable microfluidic systems. *Lab Chip*, 6, 659–666.
- 618 Guarracino, L., & Jougnot, D. (2018). A physically based analytical model to describe effective excess charge for streaming potential generation in water saturated porous media. *Journal of Geophysical Research: Solid Earth*, 123, 52–65.

⁶²² Han, S.-J., Kim, S.-S., & Kim, B.-I. (2004). Electroosmosis and pore pressure ⁶²³
development characteristics in lead contaminated soil during electrokinetic ⁶²⁴
remediation. *Geosciences Journal*, 8, 85.

⁶²⁵ Hu, G., & Li, D. (2007). Multiscale phenomena in microfluidics and nanoflu⁶²⁶
idics. *Chemical Engineering Science*, 62, 3443 – 3454.

⁶²⁷ Hu, X., Hu, S., Jin, F., & Huang, S. (2017). *Physics of Petroleum Reservoirs*.
⁶²⁸ Springer-Verlag Berlin Heidelberg.

⁶²⁹ Hunter, R. J. (1981). *Zeta Potential in Colloid Science*. Academic, New ⁶³⁰
York.

⁶³¹ Israelachvili, J. (1992). *Intermolecular and Surface Forces*. Academic Press.

⁶³² Jaafar, M. Z., Vinogradov, J., & Jackson, M. D. (2009). Measure⁶³³ment of
streaming potential coupling coefficient in sandstones satu⁶³⁴rated with
high salinity nacl brine. *Geophysical Research Letters*, 36, ⁶³⁵
doi:10.1029/2009GL040549.

⁶³⁶ Jacob, H. M., & Subirm, B. (2006). *Electrokinetic and Colloid Transport* ⁶³⁷
Phenomena. Wiley-Interscience.

⁶³⁸ Jardani, A., Revil, A., Boleve, A., Crespy, A., Dupont, J.-P., Barrash, W., & ⁶³⁹
Malama, B. (2007). Tomography of the darcy velocity from self-potential ⁶⁴⁰
measurements. *Geophysical Research Letters*, 34.

⁶⁴¹ Jougnot, D., Linde, N., Revil, A., & Doussan, C. (2012). Derivation of ⁶⁴²soil-
specific streaming potential electrical parameters from hydrodynamic ⁶⁴³
characteristics of partially saturated soils. *Vadose Zone Journal*, 11, 272– ⁶⁴⁴286.

⁶⁴⁵ Jougnot, D., Mendieta, A., Leroy, P., & Maineult, A. (2019). Exploring the ⁶⁴⁶
effect of the pore size distribution on the streaming potential generation in ⁶⁴⁷
saturated porous media, insight from pore network simulations. *Journal* ⁶⁴⁸
of Geophysical Research: Solid Earth, 124, 5315–5335.

⁶⁴⁹ Jurin, J. (1719). li. an account of some experiments shown before the royal ⁶⁵⁰
society; with an enquiry into the cause of the ascent and suspension of ⁶⁵¹water
in capillary tubes. *Philosophical Transactions of the Royal Society* ⁶⁵²
of London, 30, 739–747.

- ⁶⁵³Katz, A. J., & Thompson, A. H. (1985). Fractal sandstone pores: Implications⁶⁵⁴ for conductivity and pore formation. *Phys. Rev. Lett.*, *54*, 1325–1328.
- ⁶⁵⁵Kirby, B. (2010). *Micro and Nanoscale Fluid Mechanics: Transport in Microfluidic Devices*. Cambridge University Press.
- ⁶⁵⁷Larue, O., Wakeman, R., Tarleton, E., & Vorobiev, E. (2006). Pressure electroosmotic dewatering with continuous removal of electrolysis products.
⁶⁵⁹ *Chemical Engineering Science*, *61*, 4732 – 4740.
- ⁶⁶⁰Leroy, P., & Mainault, A. (2018). Exploring the electrical potential inside cylinders beyond the Debye-Hückel approximation: a computer code to solve the Poisson-Boltzmann equation for multivalent electrolytes.
Geophysical Journal International, *214*, 58–69.
- ⁶⁶⁴Leroy, P., & Revil, A. (2004). A triple-layer model of the surface electrochemical properties of clay minerals. *Journal of Colloid and Interface Science*, *270*, 371 – 380.
- ⁶⁶⁷Levine, S., Marriott, J., Neale, G., & Epstein, N. (1975). Theory of electrokinetic flow in fine cylindrical capillaries at high zeta-potentials. *Journal of Colloid and Interface Science*, *52*, 136 – 149.
- ⁶⁷⁰Li, S. X., Pengra, D. B., & P.Z.Wong (1995). Onsager's reciprocal relation and the hydraulic permeability of porous media. *Physical Review E*, *51*, 5748–5751.
- ⁶⁷³Liang, M., Yang, S., Miao, T., & Yu, B. (2015). Analysis of electroosmotic characters in fractal porous media. *Chemical Engineering Science*, *127*.
- ⁶⁷⁵Liang, M., Yang, S., & Yu, B. (2014). A fractal streaming current model for charged microscale porous media. *Journal of Electrostatics*, *72*.
- ⁶⁷⁷Linan Jiang, Mikkelsen, J., Jae-Mo Koo, Huber, D., Shuhuai Yao, Lian Zhang, Peng Zhou, Maveety, J. G., Prasher, R., Santiago, J. G., Kenny, T. W., & Goodson, K. E. (2002). Closed-loop electroosmotic microchannel cooling system for vlsi circuits. *IEEE Transactions on Components and Packaging Technologies*, *25*, 347–355.
- ⁶⁸²Linde, N., Binley, A., Tryggvason, A., Pedersen, L. B., & Revil, A. (2006). Improved hydrogeophysical characterization using joint inversion of cross

hole electrical resistance and ground-penetrating radar traveltime data. ⁶⁸⁵
Water Resources Research, 42.

⁶⁸⁶ Lockhart, N., & Hart, G. (1988). Electro-osmotic dewatering of fine suspen⁶⁸⁷
sions: the efficacy of current interruptions. *Drying Technology*, 6, 415–423.

⁶⁸⁸ Luong, D. T., & Sprik, R. (2013). Streaming potential and electroosmosis ⁶⁸⁹
measurements to characterize porous materials. *ISRN Geophysics, Article* ⁶⁹⁰*ID*
496352, 8 pages.

⁶⁹¹ Lyklema, J. (1995). *Fundamentals of Interface and Colloid Science*. Aca⁶⁹²
demic Press.

⁶⁹³ Mandelbrot, B. B. (1982). *The Fractal Geometry of Nature*. W.H. Freeman, ⁶⁹⁴
New York.

⁶⁹⁵ Mohiuddin Mala, G., Li, D.-D., Werner, C., Jacobasch, H.-J., & Ning, Y. ⁶⁹⁶ (1997).
Flow characteristics of water through a microchannel between two ⁶⁹⁷ parallel
plates with electrokinetic effects. *International Journal of Heat* ⁶⁹⁸ *and Fluid Flow*,
18, 489–496.

⁶⁹⁹ Nourbehecht, B. (1963). *Irreversible thermodynamic effects in inhomoge*⁷⁰⁰
neous media and their applications in certain geoelectric problems. PhD ⁷⁰¹ thesis,
MIT Press, Cambridge, Mass, USA.

⁷⁰² Ohshima, H., & Kondo, T. (1990). Electrokinetic flow between two parallel ⁷⁰³
plates with surface charge layers: Electro-osmosis and streaming potential. ⁷⁰⁴
Journal of Colloid and Interface Science, 135, 443–448.

⁷⁰⁵ Olivares, W., Croxton, T. L., & McQuarrie, D. A. (1980). Electrokinetic flow
⁷⁰⁶ in a narrow cylindrical capillary. *The Journal of Physical Chemistry*, 84, ⁷⁰⁷
867–869.

⁷⁰⁸ Ottosen, L., & Rørig-Dalgaard, I. (2006). Drying brick masonry by electro⁷⁰⁹
osmosis. In *Proceedings of the Seventh International Masonry Conference*. ⁷¹⁰
British Masonry Society.

⁷¹¹ Paillat, T., Moreau, E., P.O.Grimaud, & Touchard, G. (2000). Electroki⁷¹²
netic phenomena in porous media applied to soil decontamination. *IEEE* ⁷¹³
Transactions on Dielectrics and Electrical Insulation, 7, 693–704.

⁷¹⁴Pascal, J., Oyanader, M., & Arce, P. (2012). Effect of capillary geometry on ⁷¹⁵ predicting electroosmotic volumetric flowrates in porous or fibrous media. ⁷¹⁶ *Journal of Colloid and Interface Science*, *378*, 241 – 250.

⁷¹⁷ Pengra, D., Li, S. X., & Wong, P. (1999). Determination of rock properties ⁷¹⁸ by low frequency ac electrokinetics. *Journal of Geophysical Research*, *104*, ⁷¹⁹ 29485–29508.

⁷²⁰Pride, S. (1994). Governing equations for the coupled electromagnetics and ⁷²¹ acoustics of porous media. *Physical Review B*, *50*, 15678–15696.

⁷²² Pride, S. R., & Morgan, F. D. (1991). Electrokinetic dissipation induced by ⁷²³ seismic waves. *Geophysics*, *56*, 914–925.

⁷²⁴Quincke, G. (1861). Ueber die fortfhrung materieller theilchen durch str⁷²⁵ mende elektricit. *Annalen der Physik*, *189*, 513–598.

⁷²⁶Reddy, K. R., Parupudi, U. S., Devulapalli, S. N., & Xu, C. Y. (1997). Effects ⁷²⁷ of soil composition on the removal of chromium by electrokinetics. *Journal* ⁷²⁸ *Hazardous Materials*, *55*, 135 – 158.

⁷²⁹Reuss, F. (1809). Sur un nouvel effet de l'electricit galvanique. *Mmoires de* ⁷³⁰ *Societ Imperiale de Naturalistes de Moscou*, *2*, 327–336.

⁷³¹Revil, A., Cathles III, L. M., & Manhardt, P. D. (1999). Permeability of ⁷³² shaly sands. *Water Resources Research*, *3*, 651–662.

⁷³³Revil, A., & Leroy, P. (2004). Constitutive equations for ionic transport in ⁷³⁴ porous shales. *Journal of Geophysical Research: Solid Earth*, *109*. B03208.

⁷³⁵Revil, A., & Linde, N. (2006). Chemico-electromechanical coupling in mi⁷³⁶ croporous media. *Journal of Colloid and Interface Science*, *302*, 682 – ⁷³⁷ 694.

⁷³⁸Revil, A., Linde, N., Cerepi, A., Jougnot, D., Matthi, S., & Finsterle, S. ⁷³⁹ (2007). Electrokinetic coupling in unsaturated porous media. *Journal of* ⁷⁴⁰ *Colloid and Interface Science*, *313*, 315 – 327.

⁷⁴¹Rice, C., & Whitehead, R. (1965). Electrokinetic flow in a narrow cylindrical ⁷⁴² capillary. *J. Phys. Chem.*, *69*, 4017–4024.

⁷⁴³Sen, P. N., & Goode, P. A. (1992). Influence of temperature on electrical ⁷⁴⁴ conductivity on shaly sands. *Geophysics*, *57*, 89–96.

- ⁷⁴⁵ Singhal, V., Garimella, S. V., & Raman, A. (2004). Microscale pumping technologies for microchannel cooling systems. *Birck and NCN Publications*, ⁷⁴⁷ 57.
- ⁷⁴⁸ Smoluchowski, M. (1902). Contribution à la théorie de l'endosmose électrique ⁷⁴⁹ et de quelques phénomènes corrélatifs. *Bulletin de l'Académie des Sciences de Cracovie*, ⁷⁵⁰ 8, 182–200.
- ⁷⁵¹ Soldi, M., Guarracino, L., & Jougnot, D. (2019). An analytical effective excess charge density model to predict the streaming potential generated by unsaturated flow. *Geophysical Journal International*, ⁷⁵³ 216, 380–394.
- ⁷⁵⁴ Thanh, L., & Sprik, R. (2015). Zeta potential measurement using streaming potential in porous media. *VNU Journal of Science: Mathematics Physics*, ⁷⁵⁶ 31, 56–65.
- ⁷⁵⁷ Thanh, L. D., Jougnot, D., Van Do, P., & Van Nghia A, N. (2019). A physically based model for the electrical conductivity of water-saturated porous media. *Geophysical Journal International*, ⁷⁵⁹ 219, 866–876.
- ⁷⁶⁰ Thanh, L. D., Van Do, P., Van Nghia, N., & Ca, N. X. (2018). A fractal model for streaming potential coefficient in porous media. *Geophysical Prospecting*, ⁷⁶² 66, 753–766.
- ⁷⁶³ Tsai, N.-C., & Sue, C.-Y. (2007). Review of mems-based drug delivery and dosing systems. *Sensors and Actuators A: Physical*, ⁷⁶⁴ 134, 555 – 564.
- ⁷⁶⁵ Vennela, N., Bhattacharjee, S., & De, S. (2011). Sherwood number in porous microtube due to combined pressure and electroosmotically driven flow. *Chemical Engineering Science*, ⁷⁶⁶ 66, 6515 – 6524.
- ⁷⁶⁸ Vinogradov, J., Jaafar, M. Z., & Jackson, M. D. (2010). Measurement of streaming potential coupling coefficient in sandstones saturated with natural and artificial brines at high salinity. *Journal of Geophysical Research*, ⁷⁷¹ 115, doi:10.1029/2010JB007593.
- ⁷⁷² Wang, J., Hu, H., & Guan, W. (2016). The evaluation of rock permeability with streaming current measurements. *Geophysical Journal International*, ⁷⁷⁴ 206, 1563–1573.
- ⁷⁷⁵ Wang, J., Hu, H., Guan, W., & Li, H. (2015). Electrokinetic experimental study on saturated rock samples: zeta potential and surface conductance. *Geophysical Journal International*, ⁷⁷⁷ 201, 869–877.

- ⁷⁷⁸ Wang, X., Cheng, C., Wang, S., & Liu, S. (2009). Electroosmotic pumps and
⁷⁷⁹ their applications in microfluidic systems. *Microfluidics and Nanofluidics*, ⁷⁸⁰
6, 145–162.
- ⁷⁸¹ Wise, D. L., & Trantolo, D. J. (1994). *Remediation of Hazardous Waste* ⁷⁸²
Contaminated Soils. CRC Press.
- ⁷⁸³ Wu, R. C., & Papadopoulos, K. D. (2000). Electroosmotic flow through ⁷⁸⁴
porous media: cylindrical and annular models. *Colloids and Surfaces A: 785*
Physicochemical and Engineering Aspects, 161, 469 – 476.
- ⁷⁸⁶ Wyllie, M. R. J., & Rose, W. (1950). Some theoretical considerations related ⁷⁸⁷
to the quantitative evaluation of the physical characteristics of reservoir ⁷⁸⁸ rock
from electrical log data. *Society of Petroleum Engineers*, .
- ⁷⁸⁹ Yao, S., & Santiago, J. G. (2003). Porous glass electroosmotic pumps: theory. ⁷⁹⁰
J. Colloid Interface Sci, 268, 133–142.
- ⁷⁹¹ Yu, B., & Cheng, P. (2002). A fractal permeability model for bi-dispersed ⁷⁹²
porous media. *International Journal of Heat and Mass Transfer*, 45, 2983– ⁷⁹³
2993.
- ⁷⁹⁴ Yu, B., Lee, L. J., & Cao, H. (2001). Fractal characters of pore microstruc⁷⁹⁵ tures
of textile fabrics. *Fractals*, 09, 155–163.
- ⁷⁹⁶ Zeng, S., Chen, C. H., Mikkelsen, J. C., & Santiago, J. G. (2001). Fabrication ⁷⁹⁷
and characterization of electroosmotic micropumps. *Sens. Actuators B*, 79, ⁷⁹⁸ 107–
114.